

Supporting Information

Heteroatomic $\text{Te}_x\text{S}_{1-x}$ molecule/C nanocomposites as stable cathode materials in carbonate-based electrolytes for lithium-chalcogen batteries

Fugen Sun, Bo Zhang, Hao Tang, Zhihao Yue, Xiaomin Li, Chuanqiang Yin, and Lang Zhou**

F. Sun, B. zhang, H. Tang, Z. Yue, X. Li, C. Yin, Prof. L. Zhou
Institute of Photovoltaics, Nanchang University, 999 Qianhu Road, Nanchang 330031, China

* To whom correspondence should be addressed. E-mail: sunfugen@ncu.edu.cn;
lzhou@ncu.edu.cn

Content:

1. Computational methods

- 2. Figure S1.** The HRTEM image of the as-prepared CMK-3 sample.
- 3. Figure S2.** XRD patterns of the CMK-3 and $\text{Te}_{0.1}\text{S}_{0.9}/\text{CMK-3}$ samples.
- 4. Figure S3.** N_2 adsorption-desorption isotherms of the CMK-3 and $\text{Te}_{0.1}\text{S}_{0.9}/\text{CMK-3}$ samples.
- 5. Figure S4.** High-resolution S $2p$ and Te $4s$ spectras of the S/CMK-3 and $\text{Te}_{0.1}\text{S}_{0.9}/\text{CMK-3}$ samples.
- 6. Figure S5.** The phase diagram of sulphur-tellurium binary system.
- 7. Figure S6.** CV curves of the S/CMK-3 sample at 0.1 mV s^{-1} .
- 8. Figure S7.** Results of first principle calculations showing the most stable configurations and calculated binding energies of the S-S and Te-S species with carbons.
- 9. Figure S8.** The charge-discharge curves of the $\text{Te}_{0.05}\text{S}_{0.95}/\text{CMK-3}$ and $\text{Te}_{0.2}\text{S}_{0.8}/\text{CMK-3}$ samples at 250 mA g^{-1} .
- 10. Figure S9.** FTIR spectras of the fresh and cycled $\text{Te}_{0.1}\text{S}_{0.9}/\text{CMK-3}$ electrodes.
- 11. Figure S10.** Cycling performances of the S/CMK-3 and Te/CMK-3 samples at 250 mA g^{-1} .
- 12. Figure S11.** The theoretical capacities of the $\text{Te}_x\text{S}_{1-x}/\text{CMK-3}$ ($x=0, 0.05, 0.1, 0.2$ and 1) samples.
- 13. Figure S12.** EIS of the $\text{Te}_x\text{S}_{1-x}/\text{CMK-3}$ ($x=0.05, 0.1$ and 0.2) samples before the first cycle.
- 14. Table S1.** Comparison of our results with the previously reported works on the chalcogen-C composites

Computational methods

The first principle calculations were conducted, using Perdew-Burke-Ernzerhof (PBE) exchange-correlation functional in the framework of general gradient approximation (GGA) implemented in the DMol3 package in Materials Studio (version 7.0) of Accelrys Inc. An all-electron double numerical basis set with polarization functions (double numerical polarization (DNP) basis set) was used in this work. The convergence criteria applied for geometry optimizations were 1.0×10^{-5} au, 2.0×10^{-3} au \AA^{-1} , and 5.0×10^{-3} \AA for energy change, maximum force and maximum displacement, respectively. The threshold for self-consistent-field (SCF) density convergence was set to 1.0×10^{-6} eV and the global cutoff was set to fine. For quantitatively measuring the interaction between the CMK-3 and chalcogen-containing species, we defined the binding energy E_b as follows: $E_b = E_{\text{carbon}} + E_{\text{chalcogen}} - E_{\text{total}}$. E_{carbon} , $E_{\text{chalcogen}}$, and E_{total} represent the total energies of a polyaromatic molecule, an isolated chalcogen-containing species, and a polyaromatic molecule binding to a chalcogen-containing species, respectively.

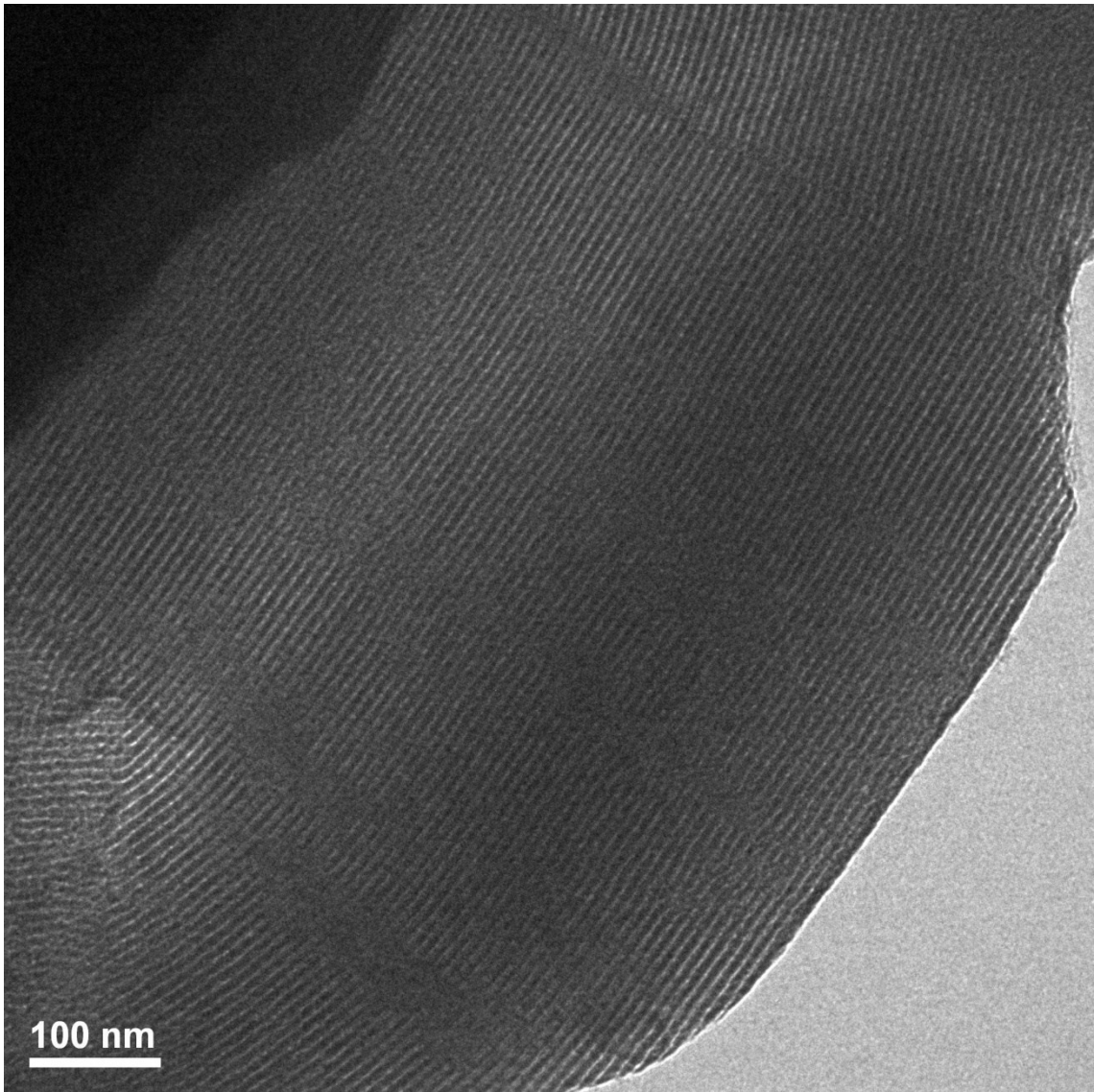


Figure S1. The HRTEM image of the as-prepared CMK-3 sample.

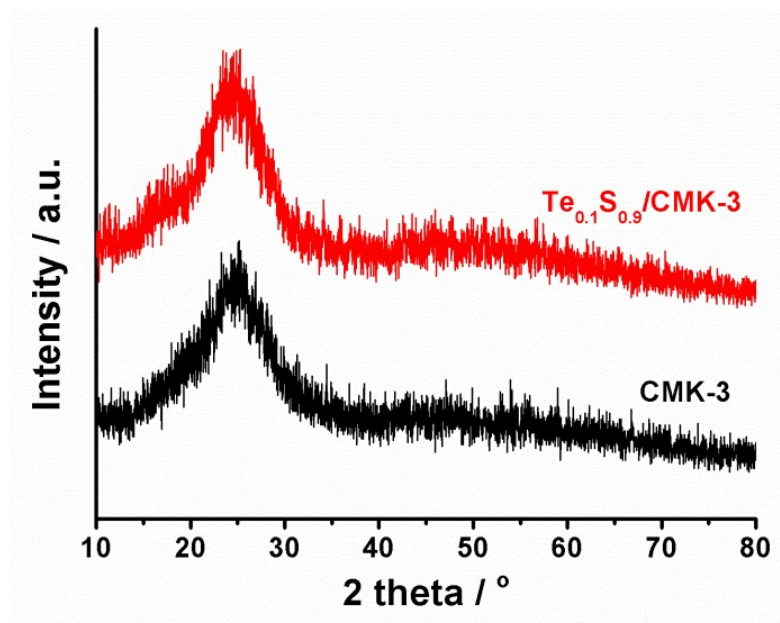


Figure S2. XRD patterns of the CMK-3 and Te_{0.1}S_{0.9}/CMK-3 samples. No distinct differences were found between the Te_{0.1}S_{0.9}/CMK-3 and CMK-3 samples, suggesting that the Te_xS_{1-x} confined in the CMK-3 are very small nanocrystal or in amorphous form.

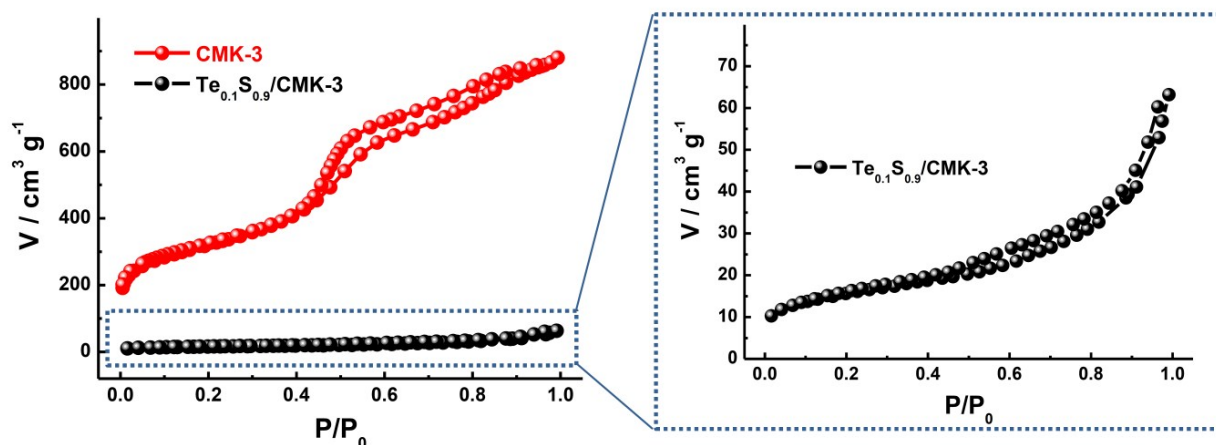


Figure S3. N_2 adsorption-desorption isotherms of the CMK-3 and $\text{Te}_{0.1}\text{S}_{0.9}/\text{CMK-3}$ samples. In comparison with the pristine CMK-3, the specific surface area, pore size and pore volume of the $\text{Te}_{0.1}\text{S}_{0.9}/\text{CMK-3}$ sample exhibit the expected decrease, demonstrating the successful incorporation of the $\text{Te}_{0.1}\text{S}_{0.9}$ into the inner surface of the mesoporous structures.

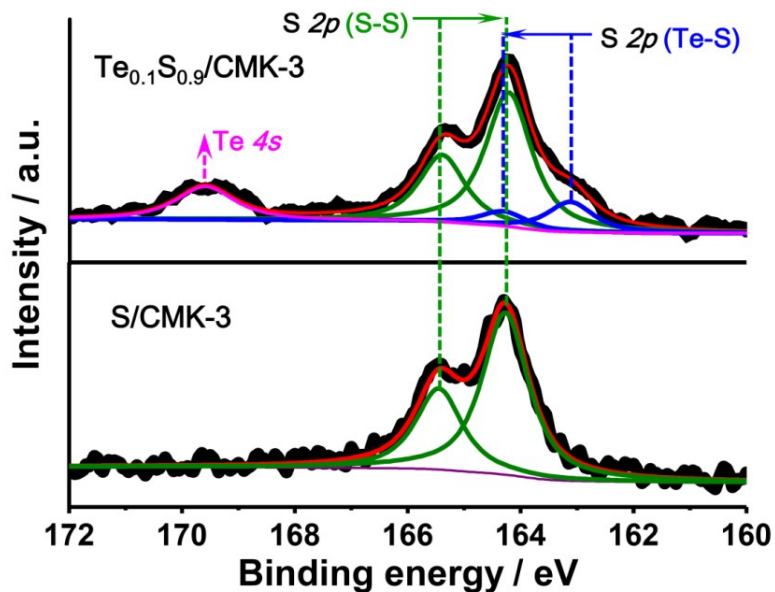


Figure S4. High-resolution S $2p$ and Te $4s$ spectra of the S/CMK-3 and $\text{Te}_{0.1}\text{S}_{0.9}/\text{CMK-3}$ samples. The S/CMK-3 sample presents characteristic S $2p_{3/2}$ and $2p_{1/2}$ peaks located at ~ 164.3 and ~ 165.5 eV for the S-S homopolar bond. However, in addition to the S-S bond, a doublet peak at a lower binding energy of $\sim 163.1/\sim 164.3$ eV, which corresponds to the Te-S heteropolar bond, was deconvoluted and curve-fitted in the $\text{Te}_{0.1}\text{S}_{0.9}/\text{CMK-3}$ sample. The presence of Te-S chemical bonding configurations in the $\text{Te}_{0.1}\text{S}_{0.9}/\text{CMK-3}$ sample further confirms the existence of tellurium sulfide compounds in them.

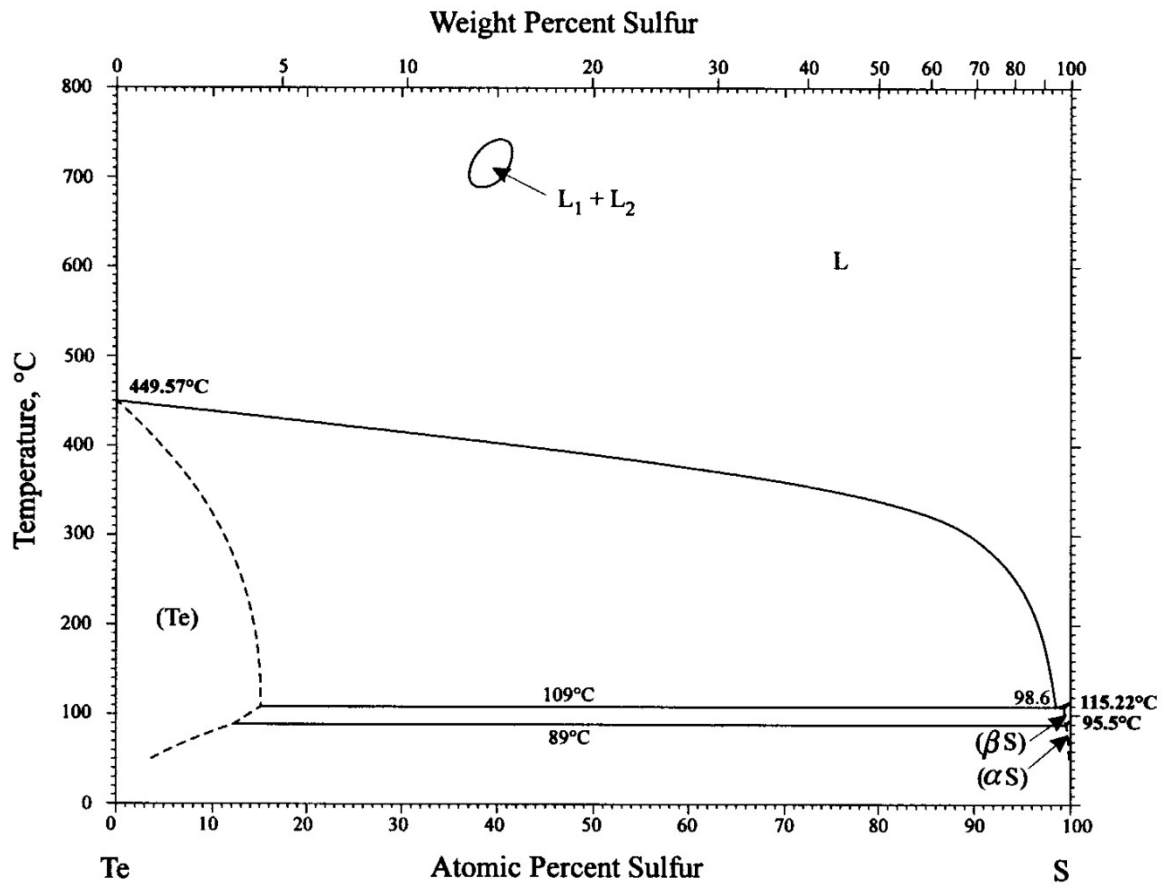


Figure S5. The phase diagram of sulphur-tellurium binary system. Reproduced with permission from Journal of Phase Equilibria. (H. Okamoto, Journal of Phase Equilibria, 1997, 18: 108)

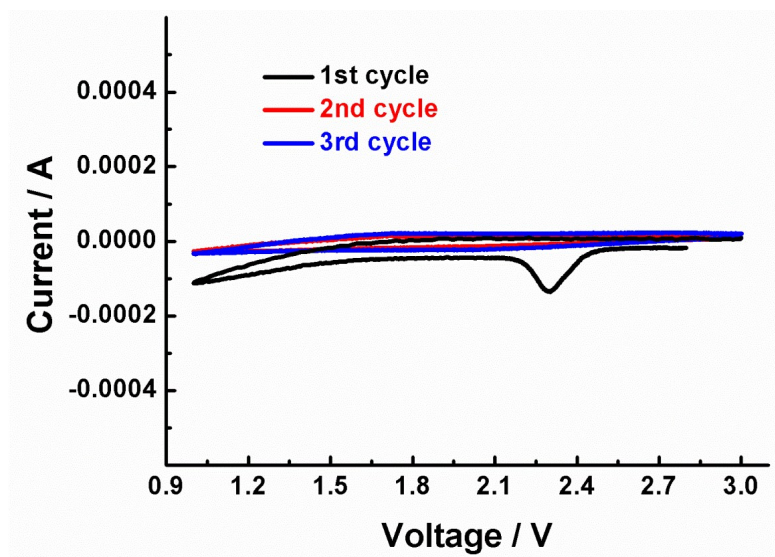


Figure S6. CV curves of the S/CMK-3 sample at 0.1 mV s^{-1} . No oxidation and reduction current peaks are observed after the first cathodic scanning of the S/CMK-3 sample. Such electrochemical incompatibility of the S/CMK-3 sample in the carbonate-based electrolytes should be due to the polysulfide consumption by an undesired chemical reaction with carbonates which occurs when the polysulfides dissolve into the electrolytes to form a single-phase solution.

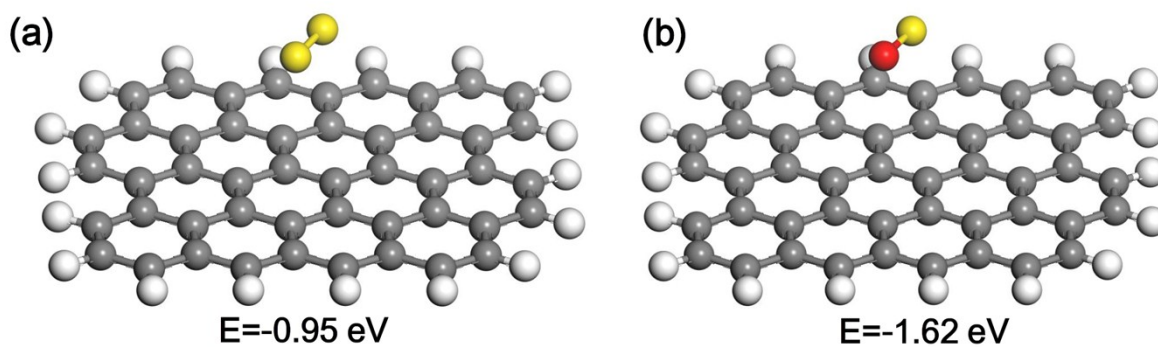


Figure S7. Results of first principle calculations showing the most stable configurations and calculated binding energies of the S-S (a) and Te-S (b) species with carbons. The black, gray, yellow and red balls represent the C, H, S and Te atoms, respectively. The CMK-3 was modeled with a single-layer carbon (typically 6 carbon rings), and the adsorption of Te-S and S-S (to represent heteroatomic tellurium sulfide and homoatomic sulfur molecules, respectively) on the carbon layer was investigated. It is found that the binding energy of heteroatomic Te-S species with carbon is stronger than that of homoatomic S-S species, which could be attributed to the higher density of polarizable electrons contributed by the larger Te atoms than S atoms.

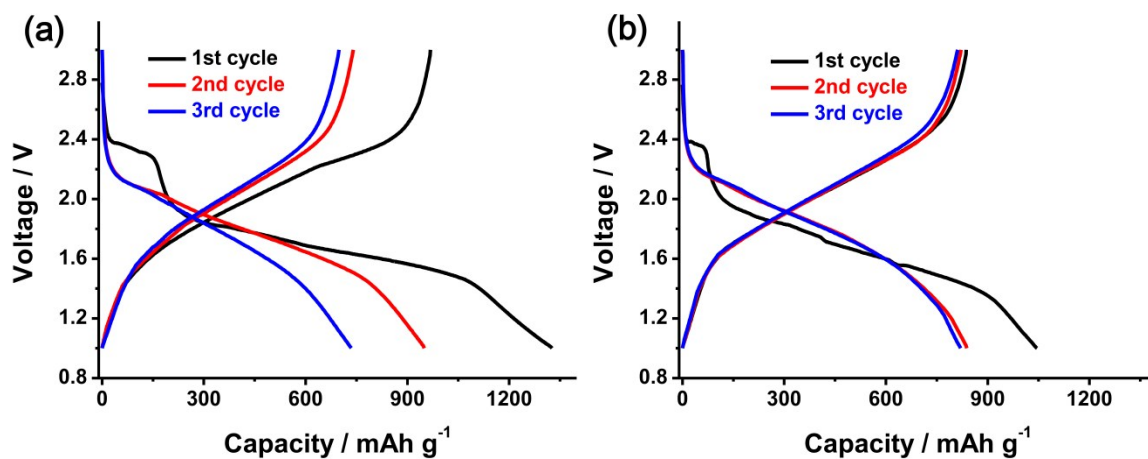


Figure S8. The charge-discharge curves of (a) the $\text{Te}_{0.05}\text{S}_{0.95}/\text{CMK-3}$ and (b) $\text{Te}_{0.2}\text{S}_{0.8}/\text{CMK-3}$ samples at 250 mA g^{-1} .

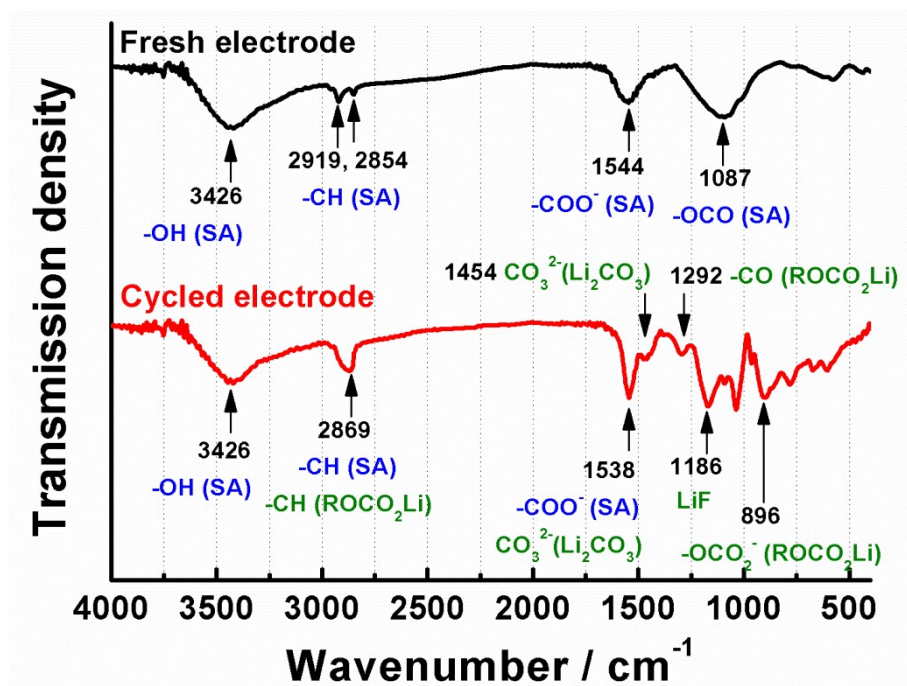


Figure S9. FTIR spectras of the fresh and cycled $\text{Te}_{0.1}\text{S}_{0.9}/\text{CMK-3}$ electrodes. In the fresh $\text{Te}_{0.1}\text{S}_{0.9}/\text{CMK-3}$ electrodes, the significant absorption peaks at 3426, 2919/2854, 1544 and 1087 cm^{-1} are mainly originated from the -OH, -CH, $-\text{COO}^-$ and -OCO bonds of the sodium alginate (SA) binder, respectively. After the first discharge-charge cycle at 3.0 V, the cycled $\text{Te}_{0.1}\text{S}_{0.9}/\text{CMK-3}$ electrodes possess new IR absorption bands, which should be resulted from the formed SEI on electrode surfaces. The absorption peak centered at 2869 cm^{-1} of the cycled $\text{Te}_{0.1}\text{S}_{0.9}/\text{CMK-3}$ electrodes should be attributed to the -CH bond of the SA and ROCO_2Li in the SEI; the peak centered at 1538 cm^{-1} should be corresponding to the $-\text{COO}^-$ bond of the SA and CO_3^{2-} of Li_2CO_3 in the SEI film. The absorption bands at 1454, 1292, 1186 and 896 cm^{-1} of the cycled $\text{Te}_{0.1}\text{S}_{0.9}/\text{CMK-3}$ electrodes should be attributed to the CO_3^{2-} of Li_2CO_3 , -CO of ROCO_2Li , LiF and $-\text{OCO}_2^-$ of ROCO_2Li in the SEI film, respectively. Therefore, it is suggesting that the composition of the formed SEI film on the cycled $\text{Te}_{0.1}\text{S}_{0.9}/\text{CMK-3}$ electrode surface includes $\text{RO}(\text{CO}_2)_2\text{Li}$, Li_2CO_3 and LiF.

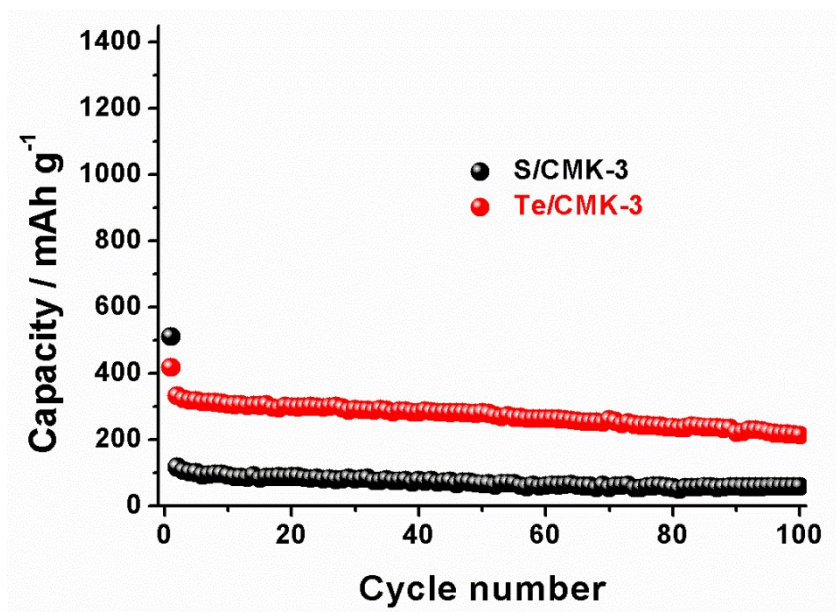


Figure 10. Cycling performances of the S/CMK-3 and Te/CMK-3 samples at 250 mA g⁻¹.

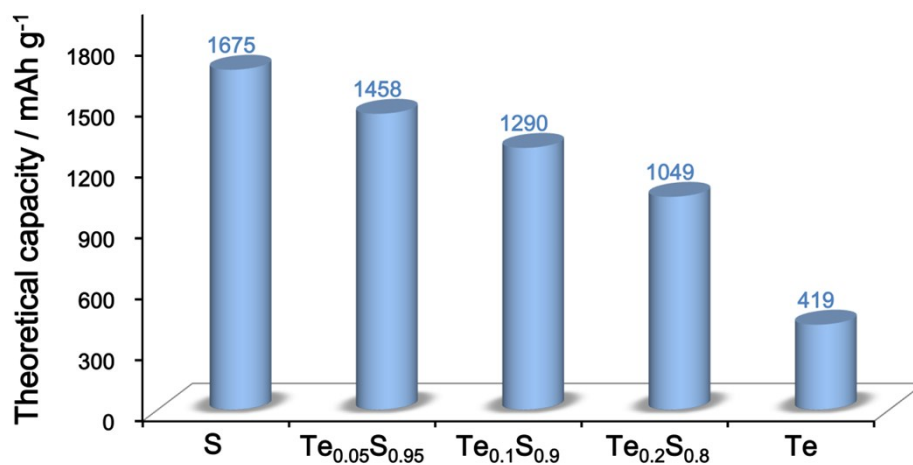


Figure S11. The theoretical capacities of the Te_xS_{1-x}/CMK-3 (x=0, 0.05, 0.1, 0.2 and 1) samples. The theoretical capacity values are calculated based on the complete reduction of Te_xS_{1-x} to Li₂S and Li₂Te.

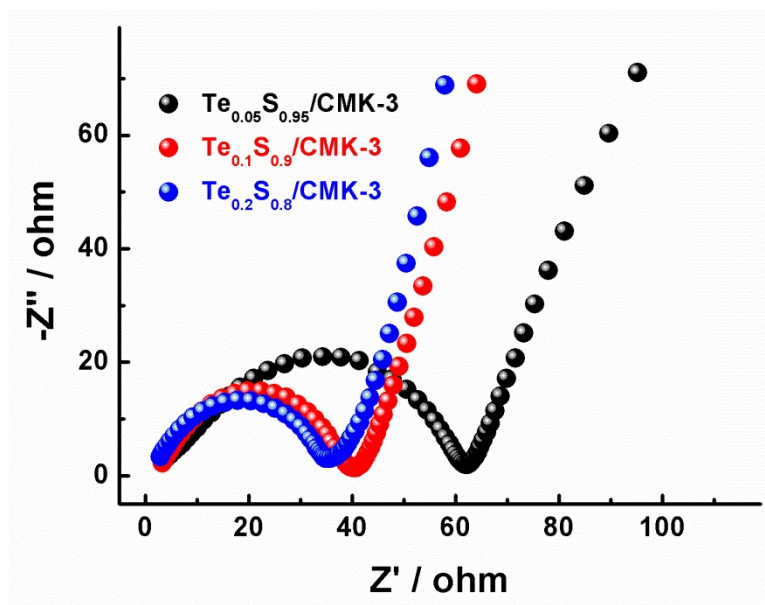


Figure S12. EIS of the $\text{Te}_x\text{S}_{1-x}/\text{CMK-3}$ ($x=0.05, 0.1$ and 0.2) samples before the first cycle. The EIS results show that the $\text{Te}_{0.1}\text{S}_{0.9}/\text{CMK-3}$ and $\text{Te}_{0.2}\text{S}_{0.8}/\text{CMK-3}$ samples have lower charge transfer resistances than that of the $\text{Te}_{0.05}\text{S}_{0.95}/\text{CMK-3}$ sample, which should be due to their improved conductivity and reaction kinetics by introducing more Te components.

Table S1. Comparison of our results with the previously reported works on the chalcogen-C composites

Composite		Electrolyte	Te _x Se _y S _z loading / wt.%	Current rate / mA g ⁻¹	The initial discharge capacity / mAh g ⁻¹ (The initial coulombic efficiency / %)	Reversible capacity / mAh g ⁻¹
S	S/NMC ¹	Ether-based electrolyte (DOL/DME)	60	335	1145 (94.1)	758 (100 cycles)
	S@CNTs/Co ₃ S ₄ -NBS ²		70	335	1535 (98.1)	1254 (100 cycles)
Se	Se/MCS ³		50	337.5	513 (92.4)	300 (100 cycles)
	Se/NDMC ⁴		56.2	675	535 (90.9)	277 (50 cycles)
Te	Te/MPC ⁵		68.0	42	670 (90.6)	391 (100 cycles) 389 (200 cycles)
			49.3	500	846 (70.5)	330 (100 cycles) 270 (200 cycles)
Se _x S _y	SeS ₂ /CMK-3@PDA ⁷		70	200	1234 (86.7)	838 (100 cycles)
			2000	777 (97.6)	545 (100 cycles) 505 (200 cycles) 350 (500 cycles)	
	SeS ₂ /HMC@TiN ⁸		70	224	987 (99.1)	840 (50 cycles) 778 (100 cycles) 690 (200 cycles)
	SeS ₂ /CoS ₂ @LRC ⁹		/	200	1015 (99.0)	745 (100 cycles)
	Se ₂ S ₅ /MMC ¹⁰		50	138.9	1565 (94.1)	346 (50 cycles)
			649.5	692 (/)	430 (100 cycles)	
	Se ₂ S ₅ /MCM ¹¹		50	337.5	1151 (95.1)	796 (100 cycles)
	Se ₂ S ₆ /NMC ¹²		60	250	1198 (96.5)	963 (50 cycles) 883 (100 cycles) 780 (200 cycles)
SeS ₇ /CNT ¹³	70	50	1540 (92.4)	833 (50 cycles)		
Te _x S _y	Te-3-S/rGO ¹⁴	66.57	5000	836 (98)	772 (100 cycles) 751 (200 cycles) 673 (500 cycles)	
S	S/CNT@MPC ¹⁵	40	167	1670 (76)	1136 (100 cycles) 1142 (200 cycles)	
		46.3	335	1404 (54.2)	353 (10 cycles)	
		50	100	813 (8.7)	30 (10 cycles)	
		57	160	1154 (65.5)	740 (50 cycles)	
Se	Se/Meso-CS ¹⁹	30	168.75	480 (34.9)	476 (100 cycles) 462 (200 cycles) 489 (500 cycles)	
		49	67.5	920 (57.8)	600 (50 cycles)	
		50	337.5	1022 (61.3)	568 (100 cycles) 570 (200 cycles)	
		51	67.5	897 (56.9)	317 (100 cycles)	
		52.3	50	663 (57)	643 (100 cycles)	
		54	100	560 (64.5)	456 (100 cycles) 433 (200 cycles)	
Se	Se/CMK-3 ²⁰	30	168.75	480 (34.9)	476 (100 cycles) 462 (200 cycles) 489 (500 cycles)	
		49	67.5	920 (57.8)	600 (50 cycles)	
		50	337.5	1022 (61.3)	568 (100 cycles) 570 (200 cycles)	
		51	67.5	897 (56.9)	317 (100 cycles)	
		52.3	50	663 (57)	643 (100 cycles)	
		54	100	560 (64.5)	456 (100 cycles) 433 (200 cycles)	
Se	Se@N-MPC ²¹	30	168.75	480 (34.9)	476 (100 cycles) 462 (200 cycles) 489 (500 cycles)	
		49	67.5	920 (57.8)	600 (50 cycles)	
		50	337.5	1022 (61.3)	568 (100 cycles) 570 (200 cycles)	
		51	67.5	897 (56.9)	317 (100 cycles)	
		52.3	50	663 (57)	643 (100 cycles)	
		54	100	560 (64.5)	456 (100 cycles) 433 (200 cycles)	
Se	Se/MC ²²	30	168.75	480 (34.9)	476 (100 cycles) 462 (200 cycles) 489 (500 cycles)	
		49	67.5	920 (57.8)	600 (50 cycles)	
		50	337.5	1022 (61.3)	568 (100 cycles) 570 (200 cycles)	
		51	67.5	897 (56.9)	317 (100 cycles)	
		52.3	50	663 (57)	643 (100 cycles)	
		54	100	560 (64.5)	456 (100 cycles) 433 (200 cycles)	
Se	Se/CNF ²³	30	168.75	480 (34.9)	476 (100 cycles) 462 (200 cycles) 489 (500 cycles)	
		49	67.5	920 (57.8)	600 (50 cycles)	
		50	337.5	1022 (61.3)	568 (100 cycles) 570 (200 cycles)	
		51	67.5	897 (56.9)	317 (100 cycles)	
		52.3	50	663 (57)	643 (100 cycles)	
		54	100	560 (64.5)	456 (100 cycles) 433 (200 cycles)	
Se	Se/PTCDA-C ²⁴	30	168.75	480 (34.9)	476 (100 cycles) 462 (200 cycles) 489 (500 cycles)	
		49	67.5	920 (57.8)	600 (50 cycles)	
		50	337.5	1022 (61.3)	568 (100 cycles) 570 (200 cycles)	
		51	67.5	897 (56.9)	317 (100 cycles)	
		52.3	50	663 (57)	643 (100 cycles)	
		54	100	560 (64.5)	456 (100 cycles) 433 (200 cycles)	

Se	Se/MPCS ²⁵	Carbonate -based electrolyte (EC/DEC)	60	67.5	926 (72.9)	540 (100 cycles)
	Se/PCS ²⁶		60	337.5	857.8 (56.5)	463 (100 cycles) 348 (200 cycles)
	Se/Micro-C ²⁷		60	675	1180 (54.4)	526 (100 cycles)
	Se/Micro-CS ²⁸		70.5	675	656 (76.4)	416 (1200 cycles)
Te	Te/PCs ²⁹		50	50	324 (30.8)	249 (100 cycles) 246 (200 cycles) 229 (500 cycles)
	Te/CMK-3 ³⁰		55.1	210	447.8 (85.7)	375 (5 cycles)
	Te/C ³¹		70	100	262 (67.5)	252 (100 cycles)
Se _x S _y	SeS _{0.7} /CPAN ³²		33	600	1269 (58.2)	827 (50 cycles) 838 (100 cycles) 838 (200 cycles) 813 (400 cycles)
	S _{0.96} Se _{0.04} @PCNF ³³		49	100	1883 (72.5)	840 (100 cycles)
	Se _{0.06} S _{0.94} /MC ³⁴		50	200	1755 (63)	1106 (50 cycles) 1077 (100 cycles) 1090 (200 cycles)
	S _{0.6} Se _{0.4} @CNFs ³⁵		57.45	100	900 (56)	450 (100 cycles)
Te _x S _y	Te _{0.1} S _{0.9} /CMK-3 (Our results)	70	250	1250 (79.1)	845 (100 cycles)	

The comparison between our results and the previously reported works demonstrate that the electrochemical performance of the Te_{0.1}S_{0.9}/CMK-3 sample is among the best series of chalcogen-based cathode materials when the key performance indicators including the reversible capacity, the initial coulombic efficiency, the Te/Se/S loading and the used electrolyte are all considered. It can be seen that in the ether-based electrolytes, S-, Se_xS_y- and Te_xS_y-based composites present higher reversible capacity than Se- and Te-based composites due to the limited theoretical gravimetric capacity of Se and Te. However, in the conventional and low-cost carbonate-based electrolytes which have been widely used in the commercial lithium-ion batteries, most of S-based composites are electrochemically incompatible and rapidly deteriorated except small S₂₋₄ molecules confined in microporous carbons with low S loading^[15]. In our present work, we first demonstrate the heteroatomic Te_xS_{1-x} molecule-based composite as an attractive cathode material in the carbonate-based electrolyte. Our results show that the heteroatomic Te_{0.1}S_{0.9}/CMk-3 composites can be reversibly charged and

discharged in the carbonate-based electrolyte with competitive cycling stability and reversible capability. Moreover, the initial coulombic efficiency and the active material loading of the heteroatomic $\text{Te}_{0.1}\text{S}_{0.9}/\text{CMk-3}$ composites are higher than most of the previously reported $\text{Se}_x\text{S}_y/\text{C}$ composites in the carbonate-based electrolytes, which are also very important to obtain high total energy density for practical applications.

References

- [1] Sun F. G.; Wang J. T.; Chen H. C.; Li W. C.; Qiao W. M.; Long D. H.; Ling L. C. High Efficiency Immobilization of Sulfur on Nitrogen-Enriched Mesoporous Carbons for Li-S Batteries. *ACS Appl. Mater. Interfaces* **2013**, *5*, 5630.
- [2] Chen T.; Zhang Z.; Cheng B.; Chen R.; Hu Y.; Ma L.; Zhu G.; Liu J.; Jin Z. Self-Templated Formation of Interlaced Carbon Nanotubes Threaded Hollow Co_3S_4 Nanoboxes for High-Rate and Heat-Resistant Lithium-Sulfur Batteries. *J. Am. Chem. Soc.* **2017**, *139*, 12710.
- [3] Liu, L.; Wei, Y.; Zhang, C.; Zhang, C.; Li, X.; Wang, J.; Ling, L.; Qiao, W.; Long, D. Enhanced Electrochemical Performances of Mesoporous Carbon Microsphere/selenium Composites by Controlling the Pore-structure and Nitrogen-doping. *Electrochim. Acta* **2015**, *153*, 140.
- [4] Qu, Y. H.; Zhang, Z. A.; Jiang, S. F.; Wang, X. W.; Lai, Y. Q.; Liu, Y. X.; Li, J. Confining Selenium in Nitrogen-containing Hierarchical Porous Carbon for High-rate Rechargeable Lithium-selenium Batteries. *J. Mater. Chem. A* **2014**, *2*, 12255.
- [5] Zhang J.; Yin Y.; You Y.; Yan Y.; Guo Y. A High-capacity Tellurium@Carbon Anode Material for Lithium-Ion Batteries. *Energy Technol.* **2014**, *2*, 757.
- [6] Zhang, Z. A.; Jiang, S. F.; Lai, Y. Q.; Li, J. M.; Song, J. X.; Li, J. Selenium Sulfide@Mesoporous Carbon Aerogel Composite for Rechargeable Lithium Batteries with Good Electrochemical Performance. *J. Power Sources* **2015**, *284*, 95.
- [7] Li Z.; Zhang J.; Wu H. B.; Lou X. W. An Improved Li- SeS_2 Battery with High Energy Density and Long Cycle Life. *Adv. Energy Mater.* **2017**, *7*, 1700281.
- [8] Li Z.; Zhang J.; Guan B. Y.; Lou X. W. Mesoporous Carbon@Titanium Nitride Hollow Spheres as an Efficient SeS_2 Host for Advanced Li- SeS_2 Batteries. *Angew. Chem.* **2017**, *129*, 16219.
- [9] Zhang J.; Li Z.; Lou X. A Free-standing Selenium Disulfide Cathode Based on Cobalt Disulfide-decorated Multichannel Carbon Fibers with Enhanced Lithium Storage Performance. *Angew. Chem., Int. Ed.* **2017**, *56*, 14107.
- [10] Xu, G. L.; Ma, T.; Sun, C. J.; Luo, C.; Cheng, L.; Ren, Y.; Heald, S. M.; Wang, C.; Curtiss, L.; Wen, J.; Miller D. J.; Li T.; Zuo X.; Petkov V.; Chen Z.; Amine K. Insight into the Capacity Fading Mechanism of Amorphous Se_2S_5 Confined in Micro/Mesoporous Carbon Matrix in Ether-Based Electrolytes. *Nano Lett.* **2016**, *16*, 2663.
- [11] Wei Y.; Tao Y.; Kong Z.; Liu L.; Wang J.; Qiao W.; Ling L.; Long D. Unique Electrochemical Behavior of Heterocyclic Selenium-Sulfur Cathode Materials in Ether-based Electrolytes for Rechargeable Lithium Batteries. *Energy Storage Materials* **2016**, *5*, 171.
- [12] Sun F.; Cheng H.; Chen J.; Zheng N.; Li Y.; Shi J. Heteroatomic $\text{Se}_n\text{S}_{8-n}$ Molecules Confined in Nitrogen-doped Mesoporous Carbons as Reversible Cathode Materials for High-Performance Lithium Batteries. *ACS Nano* **2016**, *10*, 8289.
- [13] Cui, Y.; Abouimrane, A.; Lu, J.; Bolin, T.; Ren, Y.; Weng, W.; Sun, C.; Maroni, V. A.; Heald, S. M.; Amine, K. A New Class of Lithium and Sodium Rechargeable Batteries Based on Selenium and

- Selenium-Sulfur as a Positive Electrode. *J. Am. Chem. Soc.* **2013**, *135*, 8047.
- [14] Xu K.; Liu X.; Liang J.; Cai J.; Zhang K.; Lu Y.; Wu X.; Zhu M.; Liu Y.; Zhu Y.; Wang G.; Qian Y. Manipulating the Redox Kinetics of Li-S Chemistry by Tellurium Doping for Improved Li-S Batteries. *ACS Energy Lett.* **2018**, *3*, 420.
- [15] Xin S.; Gu L.; Zhao N.; Yin Y.; Zhou L.; Guo Y.; Wan L. Smaller Sulfur Molecules Promise Better Lithium-Sulfur Batteries. *J. Am. Chem. Soc.* **2012**, *134*, 18510.
- [16] Wang L.; He X.; Li J.; Chen M.; Gao J.; Jiang C. Charge/Discharge Characteristics of Sulfurized Polyacrylonitrile Composite with Different Sulfur Content in Carbonate Based Electrolyte for Lithium Batteries. *Electrochim. Acta* **2012**, *72*, 114.
- [17] Gao J.; Lowe M. A.; Kiya Y.; Abruña H. D. Effects of Liquid Electrolytes on the Charge-discharge Performance of Rechargeable Lithium/Sulfur Batteries: Electrochemical and in-situ X-ray Absorption Spectroscopic Studies. *J. Phys. Chem. C* **2011**, *115*, 25132.
- [18] Lai C.; Gao X. P.; Zhang B.; Yan T. Y.; Zhou Z. Synthesis and Electrochemical Performance of Sulfur/Highly Porous Carbon Composites. *J. Phys. Chem. C* **2009**, *113*, 4712.
- [19] Luo, C.; Xu, Y.; Zhu, Y.; Liu, Y.; Zheng, S.; Liu, Y.; Langrock, A.; Wang, C. Selenium@Mesoporous Carbon Composite with Superior Lithium and Sodium Storage Capacity. *ACS Nano* **2013**, *7*, 8003.
- [20] Yang, C.-P.; Xin, S.; Yin, Y.-X.; Ye, H.; Zhang, J.; Guo, Y.-G. An Advanced Selenium-Carbon Cathode for Rechargeable Lithium-Selenium Batteries. *Angew. Chem., Int. Ed.* **2013**, *52*, 8363.
- [21] Jiang, Y.; Ma, X.; Feng, J.; Xiong, S. Selenium in Nitrogen-doped Microporous Carbon Spheres for High-performance Lithium-Selenium Batteries. *J. Mater. Chem. A* **2015**, *3*, 4539.
- [22] Liu, Y. X.; Si, L.; Zhou, X. S.; Liu, X.; Xu, Y.; Bao, J. C.; Dai, Z.H. A Selenium-confined Microporous Carbon Cathode for Ultrastable Lithium-Selenium Batteries. *J. Mater. Chem. A* **2014**, *2*, 17735.
- [23] Zeng, L.; Zeng, W.; Jiang, Y.; Wei, X.; Li, W.; Yang, C.; Zhu, Y.; Yu, Y. A Flexible Porous Carbon Nanofibers-Selenium Cathode with Superior Electrochemical Performance for Both Li-Se and Na-Se Batteries. *Adv. Energy Mater.* **2015**, *5*, 1401377.
- [24] Luo, C.; Wang, J.; Suo, L.; Mao, J.; Fan, X.; Wang, C. In Situ Formed Carbon Bonded and Encapsulated Selenium Composites for Li-Se and Na-Se Batteries. *J. Mater. Chem. A* **2015**, *3*, 555.
- [25] Ye, H.; Yin, Y. X.; Zhang, S. F.; Guo, Y. G. Advanced Se-C Nanocomposites: A Bifunctional Electrode Material for Both Li-Se and Li-ion Batteries. *J. Mater. Chem. A* **2014**, *2*, 13293.
- [26] Li, Z.; Yin, L. MOF-derived, N-doped, Hierarchically Porous Carbon Sponges as Immobilizers to Confine Selenium as Cathodes for Li-Se Batteries with Superior Storage Capacity and Perfect Cycling Stability. *Nanoscale* **2015**, *7*, 9597.
- [27] Yi, Z.; Yuan, L.; Sun, D.; Li, Z.; Wu, C.; Yang, W.; Wen, Y.; Shan, B.; Huang, Y. High-performance Lithium-Selenium Batteries Promoted by Heteroatom-doped Microporous Carbon. *J. Mater. Chem. A* **2015**, *3*, 3059.
- [28] Li, Z.; Yuan, L.; Yi, Z.; Liu, Y.; Huang, Y. Confined Selenium within Porous Carbon Nanospheres as Cathode for Advanced Li-Se Batteries. *Nano Energy* **2014**, *9*, 229.
- [29] Liu Y.; Wang J.; Xu Y.; Zhu Y.; Bigiob D.; Wang C. Lithium-Tellurium Batteries Based on Tellurium/Porous Carbon Composite. *J. Mater. Chem. A* **2014**, *2*, 12201.
- [30] Koketsu T.; Paul B.; Wu C.; Kraehnert R. Huang Y.; Strasser P. A Lithium-Tellurium Rechargeable Battery with Exceptional Cycling Stability. *J Appl. Electrochem.* **2016**, *46*, 627.
- [31] Seo J. U.; Seong G. K.; Park C. M. Te/C Nanocomposites for Li-Te Secondary Batteries. *Sci. Rep.* **2015**, *5*, 7969.
- [32] Luo, C.; Zhu, Y.; Wen, Y.; Wang, J.; Wang, C. Carbonized Polyacrylonitrile-stabilized SeS_x Cathodes for Long Cycle Life and High Power Density Lithium Ion Batteries. *Adv. Funct. Mater.* **2014**, *24*,

4082.

- [33] Zeng L.; Yao Y.; Shi J.; Jiang Y.; Li W.; Gu L.; Yu Y. A Flexible $S_{1-x}Se_x$ @Porous Carbon Nanofibers ($x \leq 0.1$) Thin Film with High Performance for Li-S Batteries and Room-temperature Na-S Batteries. *Energy Storage Materials* **2016**, *5*, 50
- [34] Li, X.; Liang, J.; Zhang, K.; Hou, Z.; Zhang, W.; Zhu, Y.; Qian, Y. Amorphous S-Rich $S_{1-x}Se_x/C$ ($x \leq 0.1$) Composites Promise Better Lithium-Sulfur Batteries in a Carbonate-based Electrolyte. *Energy Environ. Sci.* **2015**, *8*, 3181.
- [35] Yao Y.; Zeng L.; Hu S.; Jiang Y.; Yuan B.; Yu Y. Binding $S_{0.6}Se_{0.4}$ in 1D Carbon Nanofiber with C-S Bonding for High-performance Flexible Li-S Batteries and Na-S Batteries. *Small* **2017**, *13* (19), 1603513.